Available online at www.sciencedirect.com
ScienceDirect
European Journal of Pharmaceutics and Biopharmaceutics 69 (2008) 43–53
European Journal of Pharmaceutics and Biopharmaceutics
www.elsevier.com/locate/ejpb

Research paper

In vivo photodynamic activity of photosensitizer-loaded nanoparticles: Formulation properties, administration parameters and biological issues involved in PDT outcome

Angelica Vargas [a], Michael Eid [b], Mohammed Fanchaouy [c], Robert Gurny [a], Florence Delie [a,*]

[a] *Department of Pharmaceutics and Biopharmaceutics, University of Geneva, University of Lausanne, Switzerland*
[b] *Department of Educational Sciences and Psychology, Free University of Berlin, Germany*
[c] *Department of Zoology and Animal Biology, University of Geneva, Switzerland*

Received 5 May 2007; accepted in revised form 26 September 2007
Available online 12 October 2007

Abstract

Encapsulation of hydrophobic photosensitizers (PS) into polymeric nanoparticles (NP) has proven to be an effective alternative to organic solvents for their formulation. As NP size controls NP passage through endothelial barriers, it is a key parameter for achieving passive targeting of cancer tissues and choroidal neovascularization, secondary to age-related macular degeneration, the main applications of photodynamic therapy. In the present study, a hydrophobic PS, the *meso*-tetra(*p*-hydroxyphenyl)porphyrin, was encapsulated into biodegradable NP made of poly(D,L-lactide-co-glycolide) 50:50 via an emulsification-diffusion technique. NP batches having mean diameters of 117, 285, and 593 nm were obtained with narrow size distribution. Using the chorioallantoic membrane (CAM) of the developing chick embryo, it was demonstrated that the increase in the NP size decreased photodynamic activity *in vivo*. The activity of PS-loaded NP was not influenced by the volume of injection and was kept intact at least 6 h after NP reconstitution. Investigation of NP circulation after IV administration by fluorescence measurements revealed that 117 nm NP reached T_{max} earlier than larger NP. Confocal imaging of CAM vessels demonstrated PS uptake by endothelial cells after NP administration. It was concluded that NP size controls the photodynamic activity of the encapsulated PS.

Keywords: Photodynamic therapy; Polymeric nanoparticles; Nanoparticle size; Chick chorioallantoic membrane (CAM) model; Photosensitizer; *In vivo*; Vascular occlusion; Endothelial cells; Age-related macular degeneration; Cancer

1. Introduction

Photodynamic therapy (PDT) is an innovative alternative to conventional therapies against cancer [1], and the treatment of choroidal neovascularization (CNV), secondary to age-related macular degeneration (AMD), one of the leading causes of blindness in elderly people in developed countries [2]. PDT is based on the systemic or topical administration of photosensitizing drugs, also known as photosensitizers (PS). After biodistribution of the drug, the target tissue is illuminated with light at an appropriate wavelength and dose. Light activates the PS, which, in the presence of molecular oxygen, generates oxidizing species such as singlet oxygen. Such highly cytotoxic species induce cellular damage leading to cell death and alteration of the vasculature in terms of occlusion, stasis and/or increase in vascular permeability [1,3]. The clinical efficacy of PDT is often impeded by the difficulty in administering mostly hydrophobic PS intravenously (IV), and the low selectivity towards target tissues. Biodegradable

* Corresponding author. Department of Pharmaceutics and Biopharmaceutics, School of Pharmaceutical Sciences, University of Geneva, University of Lausanne, 30, Quai Ernest Ansermet, CH-1211 Geneva 4, Switzerland. Tel.: +41 22 379 65 73; fax: +41 22 379 65 67.
E-mail address: Florence.delie@pharm.unige.ch (F. Delie).

0939-6411/$ - see front matter © 2007 Elsevier B.V. All rights reserved.
doi:10.1016/j.ejpb.2007.09.021

nanoparticles (NP) have been proposed as a promising approach to overcome these problems [4].

In vivo studies, recently performed in our group on the chick embryo, demonstrated that the encapsulation of a hydrophobic derivative of a porphyrin into polymeric biodegradable NP allowed the IV administration of the PS [5]. Furthermore, an enhancement of the photodynamic activity of the porphyrin was observed, in terms of the occlusion of blood vessels in the chick embryo chorioallantoic membrane (CAM).

The size of colloidal drug carriers has been shown to govern their passage from the intra- to the extravascular compartment, namely extravasation [6,7]. Therefore, PS extravasation could be controlled by the size of NP in which the PS is incorporated. This strategy could be useful for achieving passive targeting of PS to either cancer tissues or the pathological choroidal neovasculature in AMD. Since the target tissues are different in cancer and CNV–AMD treatments, the optimal NP size differs between both applications, as explained below.

In the case of cancer, NP extravasation is necessary to enrich tumoral tissues in PS, thus increasing PDT outcome. Tumor tissues are characterized by a phenomenon known as enhanced permeability and retention (EPR) effect induced by leaky tumor vasculature and poor lymphatic drainage [8]. The EPR effect results in the accumulation and retention of macromolecules in the perivascular regions of solid tumors to a greater extent than in normal tissues. NP capable of crossing the fenestrations of tumoral capillaries, but large enough to be retained within the interstitial space, are a promising strategy for cancer treatment [4,9].

On the contrary, in CNV–AMD treatment by PDT, NP must be confined within the pathological neovasculature to selectively occlude the neovessels without harming the neighboring tissues, such as the retinal pigmented epithelia or the photoreceptors, failing which, further vision loss can occur. Since choroidal neovasculature exhibits hyper-permeability [10], medium- or large-sized NP that stay inside the choroidal neovasculature would be useful to protect healthy surrounding tissues against phototoxicity.

The objective of this study was to optimize NP with respect to the above-mentioned pathologies. NP of different sizes incorporating a hydrophobic PS were developed, and their *in vivo* activity, in terms of light-induced vascular occlusion, was assessed in the CAM model. The CAM model offers several advantages for the *in vivo* evaluation of PS [11,12]. CAM has a well vascularized membrane, which is easily accessible and easy to handle for PS administration, light irradiation, fluorescence analysis of administered PS, and optical examination of PDT-induced vascular damage [11,12]. Apart from the NP size, some important parameters for potential use in clinics, such as the volume of solvent used for administering a given dose of PS and the effect of NP resuspension after freeze-drying, were evaluated. Furthermore, biological issues related to the NP size, such as the residence time of the NP within the vascular compartment and the uptake of NP by vascular endothelial cells, were investigated.

2. Materials and methods

2.1. Chemicals

Poly(D,L-lactide-co-glycolide) (PLGA) with a copolymer ratio of 50:50 and molecular weight of 12 kDa (Resomer® RG502) was obtained from Boehringer Ingelheim (Ingelheim, Germany). Poly(vinyl alcohol) (PVAL) 87.7% hydrolyzed, with a molecular weight of 26 kDa (Mowiol® 4–88), was obtained from Hoechst (Frankfurt/Main, Germany). Polyethyleneglycol 400 Ph. Eur. (PEG 400) was provided by Merck (Schuchardt, Germany). Concanavalin A labelled with fluorescein isothiocyanate (FITC-Con A), meso-tetra(*p*-hydroxyphenyl)porphyrin (which will be referred to as *m*-THPP), NaCl, phosphate-buffered saline (PBS), and D(+)-trehalose dihydrate were provided by Sigma–Aldrich (Steinheim, Germany). Benzyl alcohol, ethanol 99.8%, propylene carbonate and rhodamine 101 were obtained from Fluka (Buchs, Switzerland), as well as the chemicals used to prepare HEPES-buffered saline: dextrose, HEPES, sodium chloride, sodium phosphate dibasic dihydrate and potassium chloride. All chemicals were of analytical grade and were used without further purification.

2.2. Nanoparticle preparation

PLGA NP of three different sizes loaded with *m*-THPP were prepared using the emulsification-diffusion technique as previously described [5,13]. The experimental conditions for obtaining NP of around 100, 300 and 600 nm were determined after preliminary experimentation and are summarized in Table 1. In a typical procedure, PLGA and *m*-THPP were dissolved in a mixture of benzyl alcohol and propylene carbonate. Three grams of this organic phase was added to 4 g of an aqueous phase containing PVAL and mechanically stirred to form an oil-in-water nanoemulsion. After 15 min of stirring, 500 ml of distilled water was added to the emulsion to induce the formation of the NP after complete diffusion of the organic solvents into the aqueous external phase. Mechanical stirring (2000 rpm) was maintained for 10 min. NP were purified by cross-flow filtration as described previously [13]. Purified NP were freeze-dried in the presence of trehalose (trehalose/NP mass ratio 2:1) with a freeze-dryer Lyolab C II (LSL Secfroid, Aclens, Switzerland).

2.3. Nanoparticle characterization

The mean diameter and the polydispersity index of the freeze-dried NP were determined by photon correlation spectroscopy, and the zeta potential of NP in 10 mM NaCl was measured using the technique of electrophoretic laser Doppler anemometry (Zetasizer® 5000, Malvern,

Table 1
Experimental conditions used to produce nanoparticles of different sizes via the emulsification-diffusion technique

Batch	Stirring rate[a] (rpm)	Aqueous phase	Organic phase (% w/w)			
		PVAL (% w/w)	Benzyl alcohol	Propylene carbonate	PLGA	*m*-THPP
NP 100	2000	17.0	70.0	22.3	7.0	0.7
NP 300	2000	9.0	70.0	24.5	5.0	0.5
NP 600	1500	6.0	70.0	21.2	8.0	0.8

[a] During the emulsification step.

Worcestershire, UK). The NP size and shape were checked by scanning electron microscopy (JEOL JSM-6400, Jeol Ltd., Japan). The residual PVAL remaining on the surface of purified NP was determined by a colorimetric method as previously described [13]. To determine drug loading, freeze-dried NP were suspended into 2 N NaOH under magnetic stirring for 1 h to promote PLGA hydrolysis. Then, the *m*-THPP content was determined spectrophotometrically at 688 nm with a Cintra 40 spectrometer (GBC, Victoria, Australia). Fluorescence emission spectra of *m*-THPP formulations were obtained with a Fluoromax spectrofluorometer (Spex, Stanmore, UK).

2.4. Chick chorioallantoic membrane (CAM) assay

For CAM assay, the procedure of Lange et al. [11] was adopted with minor modifications. The evaluation of *m*-THPP formulations with the CAM model is represented in Fig. 1.

2.4.1. *m*-THPP formulations

Four formulations were evaluated: three batches of NP (100, 300 and 600 nm) suspended in isotonic PBS, and free *m*-THPP (solution in water, PEG 400 and ethanol 5:3:2 v/v/v).

2.4.2. Egg incubation and CAM preparation

Fertilized hen eggs were incubated until the CAM assay at day 12 of incubation as described previously [5]. The eggshell was opened to access the CAM vasculature.

2.4.3. Microscope setup

Microscopic observations of CAM vasculature and the light irradiation during PDT were performed with an Eclipse 600 FN microscope equipped with a 4×/0.1 CFI achromat objective (Nikon, Tokyo, Japan). Illumination was provided by a 100-W mercury arc lamp. Light doses were adjusted with neutral density filters and measured with a calibrated FieldMaster power meter (Coherent, Santa Clara, USA). For

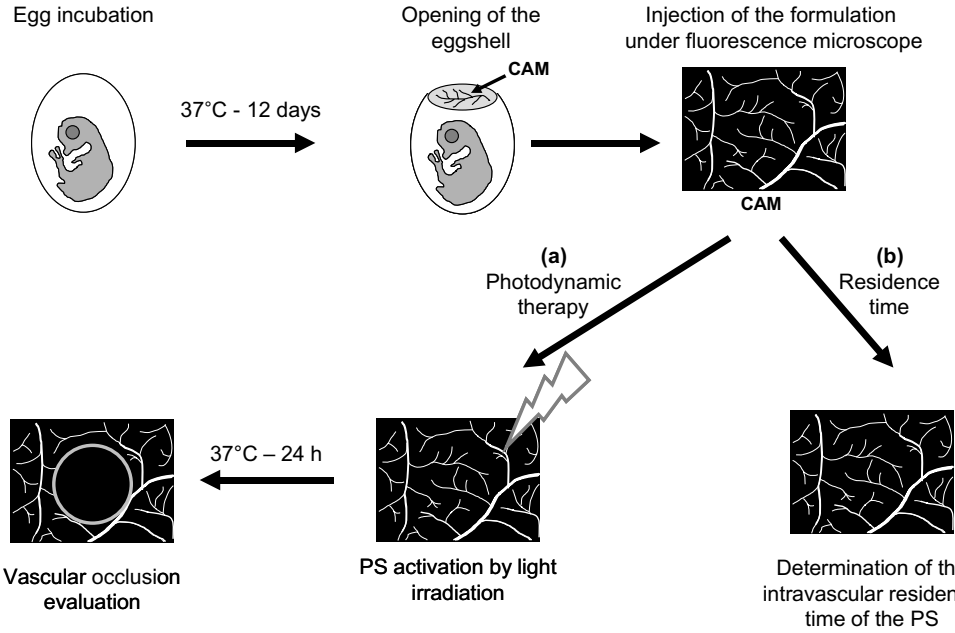

Fig. 1. Evaluation of *m*-THPP formulations with the CAM model. Fertilized eggs are incubated for 12 days, when the eggshell is opened to access the CAM. After transferring the eggs under the objective of a fluorescence microscope, *m*-THPP formulations are administered to the embryo by IV injection. Then, it is possible to perform photodynamic therapy experiments (a), or to determine the intravascular residence time of the PS (b). PDT is performed by irradiating the membrane with filtered light from the fluorescence microscope. Then, 24 h post-PDT, vascular occlusion is assessed after injection of a fluorescent compound (rhodamine 101). The intravascular residence time of *m*-THPP is determined from angiographies taken at different time-points after administration using the fluorescence emitted by *m*-THPP.

detecting *m*-THPP, the microscope was equipped with a BV-2A cube (Nikon, Tokyo, Japan) and an additional 650/50 nm band-pass filter (Chroma Technology Corp., Rockingham, USA). For detecting rhodamine 101, a G-2B cube was used (Nikon, Tokyo, Japan). Fluorescence angiographies were acquired with a cooled Retiga EX CCD digital camera (Qimaging, Burnaby, Canada) and processed using Openlab version 3.1.5 software (Improvision, Coventry, UK).

2.4.4. Photodynamic therapy and evaluation of vascular occlusion

PDT assays were performed as described previously [5]. Briefly, *m*-THPP formulations were injected into one of the main blood vessels of CAM, and the PS was activated with light from the Eclipse 600 FN microscope. In a typical experiment, 1 min after the IV injection of the formulations, a CAM region (1.8 mm^2) was irradiated to achieve a light dose of 15 J/cm^2 at 420 nm. To document vascular effects of the photodynamic treatment, fluorescence angiography of the irradiated area was performed 24 h after treatment by injecting rhodamine 101 (0.5 mg/kg). Comparison of angiographies taken before and 24 h after PDT allowed the evaluation of vascular occlusion, using an arbitrary damage scale ranked from 0 to 5 proposed by Lange et al. (Table 2) [11]. The "0" rank corresponds to no vascular occlusion and "5" to the maximum photodynamic effect, where complete occlusion of all the vessels in the irradiated area is achieved. The following parameters were evaluated: (i) the formulation type; (ii) the injection volume (10 or 20 μl); and (iii) the delay between formulation reconstitution and administration. In this case, formulations were administered immediately post-reconstitution, or kept in the dark at room temperature and administered 6 or 24 h post-reconstitution.

2.4.5. Graphical representation and statistical analysis of PDT experiments

For graphical representation, each set of data corresponding to seven experiments performed in different embryos was represented by the median and the median absolute deviation (MAD). The arbitrary scale used to score vascular occlusion in CAM experiments is ordinal, thus non-parametric statistical tests were employed to compare the data. The Mann–Whitney *U* test was used to compare two independent samples, whereas the Kruskal–Wallis *H* test was used to analyze several independent samples using the SPSS 14.0 software (SPPS Inc., Chicago, USA). To test the hypotheses, exact tests were performed. In the case of multiple post-hoc comparisons, the *p*-values were corrected by a Bonferroni correction. All hypotheses were tested according to an α-level of 0.05.

2.4.6. Residence time of m-THPP within the intravascular compartment

Since *m*-THPP is a fluorescent compound, its localization in the CAM (either intra- or extra-vascular) can be determined by fluorescence angiography of CAM vessels. The intensity of PS fluorescence inside and outside vessels thus allows to estimate PS extravasation after administration, as described before [11]. After injecting 20 μl of *m*-THPP formulations into chick embryos (1.2 mg/kg), fluorescence angiographies were taken several times during a period of 25 min. The photographic contrast (C_{phot}) for each time-point was calculated as proposed by Lange et al. (Eq. 1) [11]. C_{phot} as a function of time allows expressing the evolution of fluorescence intensity in blood vessels (I_{in}) in relation to the surrounding tissue (I_{out}) for each embryo.

$$C_{phot} = \frac{(I_{in} - I_{out})}{(I_{in} + I_{out})} \quad (1)$$

Then, the C_{phot} was normalized by the maximum photographic contrast obtained per embryo after administration ($C_{phot.max}$) (Eq. 2).

$$\text{Normalized } C_{phot} = \frac{C_{phot}}{C_{phot.\ max}} \quad (2)$$

Four embryos were evaluated for each formulation, and the normalized C_{phot} was plotted as a function of time. The time at which the $C_{phot.max}$ was reached will be referred to as T_{max}.

2.5. Confocal microscopy of CAM blood vessels after m-THPP administration

Ten minutes after the administration of *m*-THPP formulations to chick embryos (2.5 mg/kg in 20 μl), the main artery of CAM was resected from the membrane and introduced into a Petri dish containing HEPES-buffered saline (HBS). Under a stereoscope, the vessel was longitudinally opened and fixed to a transparent polymeric support with the tunica intima side up. The excised tissue was washed 3 times with HBS to remove residual blood. Freshly prepared

Table 2
Evaluation of PDT-induced damage on CAM vessels [11]

Scale	Criterion
0	No vascular occlusion
1	Partial closure of capillaries of diameter (d) <10 μm
2	Closure of capillary system, partial closure of vessels ($d < 30$ μm) and size reduction of larger vessels
3	Closure of vessels ($d < 30$ μm) and partial closure of larger vessels
4	Total closure of vessels ($d < 70$ μm) and partial closure of larger vessels
5	Total occlusion of vessels in the irradiated area

FITC-Con A in HBS (200 μg/ml) was added to the Petri dish to allow staining of endothelial cell membranes for 10 min. The tissue was then washed 6 times with HBS, and confocal microscopy images were obtained with an Axioplan 2 microscope coupled to a LSM 510 META laser unit, using a 40×/0.8 Achroplan objective (Carl Zeiss, Jena, Germany). Fluorescent signals were simultaneously recorded as follows: for FITC $\lambda_{excitation}$ 488 nm and $\lambda_{emission}$ 505–530 nm, and for *m*-THPP $\lambda_{excitation}$ 405 nm and $\lambda_{emission}$ 636–753 nm. Three embryos were evaluated per formulation.

3. Results

3.1. Preparation and characterization of nanoparticles

NP of three different sizes were obtained via the emulsification-diffusion technique. NP characteristics are summarized in Table 3. Mean diameters were 117, 285, and 593 nm. These batches will be hereafter referred to as 100, 300 and 600 nm NP, respectively. The variation of the PVAL concentration in the aqueous phase, as well as the stirring rate, allowed to control the NP size (Table 1). NP of around 100 nm were obtained by using high concentration of PVAL in the aqueous phase (17% w/w). Larger NP were obtained with lower PVAL concentrations. The NP size polydispersity was low (polydispersity index < 0.1). The homogeneity of the NP size and shape was checked by electron microscopy (data not shown). The zeta potentials of the three batches were close to each other (-1.7 ± 0.5 mV; mean ± SD). Although NP were purified by cross flow filtration using 12 L of water per batch, it was not possible to eliminate all the residual PVAL from NP surfaces. Residual PVAL dramatically decreased as a function of size from 22.5% to 3.0% w/w for 100 and 600 nm NP, respectively. Drug loading was around 9% w/w, but slightly increased with increasing the NP size. Nevertheless, the *m*-THPP/PLGA ratio for the three NP batches remained constant.

3.2. Influence of the formulation properties and administration parameters on the photodynamic efficacy of m-THPP

The extent of vascular occlusion induced by *m*-THPP upon light irradiation was evaluated by measuring the diameter of the occluded blood vessels and assigning a score (Table 2), as proposed by Lange et al. [11]; typical examples are shown in Fig. 2. The photodynamic activity of *m*-THPP formulations is summarized in Fig. 3. Vascular occlusion for free *m*-THPP was similar to that of 100 nm NP and increased with the dose up to 2.5 mg/kg. Although the three formulations of NP had similar *m*-THPP loadings and *m*-THPP/PLGA ratios (Table 3), the phototoxic activity of the drug significantly decreased with increasing NP size (Fig. 3).

The influence of the injection volume on the activity of *m*-THPP is shown in Fig. 4. The injected volume did not influence the activity of 100 and 300 nm NP. However, this change significantly influenced the activity of free *m*-THPP: the extent of vascular occlusion was significantly higher when 20 μl was injected.

In order to assess the influence of the delay between the reconstitution of formulations and administration, *m*-THPP formulations were administered to chick embryos immediately, 6 or 24 h after reconstitution, and the results are summarized in Fig. 5. When injected 6 h after reconstitution, the phototoxic activity was not significantly different from the activity observed when the injection was made immediately after the reconstitution of the formulations. Twenty-four hours after reconstitution, the activity of 100 and 300 nm NP decreased significantly compared to that of the fresh suspension, whereas the activity of free *m*-THPP and 600 nm NP was unaffected. The absorption spectra of 300 nm NP registered immediately and 24 h after reconstitution are shown in Fig. 6a. When NP were administered 24 h post-reconstitution, fluorescent spots were observed in the angiographies (Fig. 6b).

3.3. Influence of biological issues on the photodynamic efficacy of m-THPP

3.3.1. Residence time of m-THPP within the intravascular compartment

Fluorescence emission spectra of *m*-THPP loaded in the NP were recorded to assess the effect of encapsulation on the fluorescence quantum yield of *m*-THPP. Although *m*-THPP fluorescence ($\lambda_{excitation}$ 420 nm) was still observed, its intensity decreased when NP size increased (Fig. 7).

Table 3
Characterization of *m*-THPP-loaded nanoparticles after lyophilization

Batch	Actual size[a] (nm)	P.I.[b]	Nanoparticle composition (% w/w)			*m*-THPP/PLGA ratio (% w/w)	Zeta potential[a] (mV)
			PVAL	*m*-THPP	PLGA[c]		
NP 100	117 ± 8	0.04	22.5	7.8	69.7	11.2	−2.2 ± 0.3
NP 300	285 ± 7	0.05	7.0	8.7	84.3	10.3	−1.2 ± 0.5
NP 600	593 ± 15	0.08	3.0	9.5	87.5	10.9	−1.8 ± 0.2

[a] $n = 3$, determined on one single batch.
[b] P.I.: Polydispersity index; scale from 0 to 1.
[c] Calculated by subtraction of PVAL and *m*-THPP contents from NP dried weight.

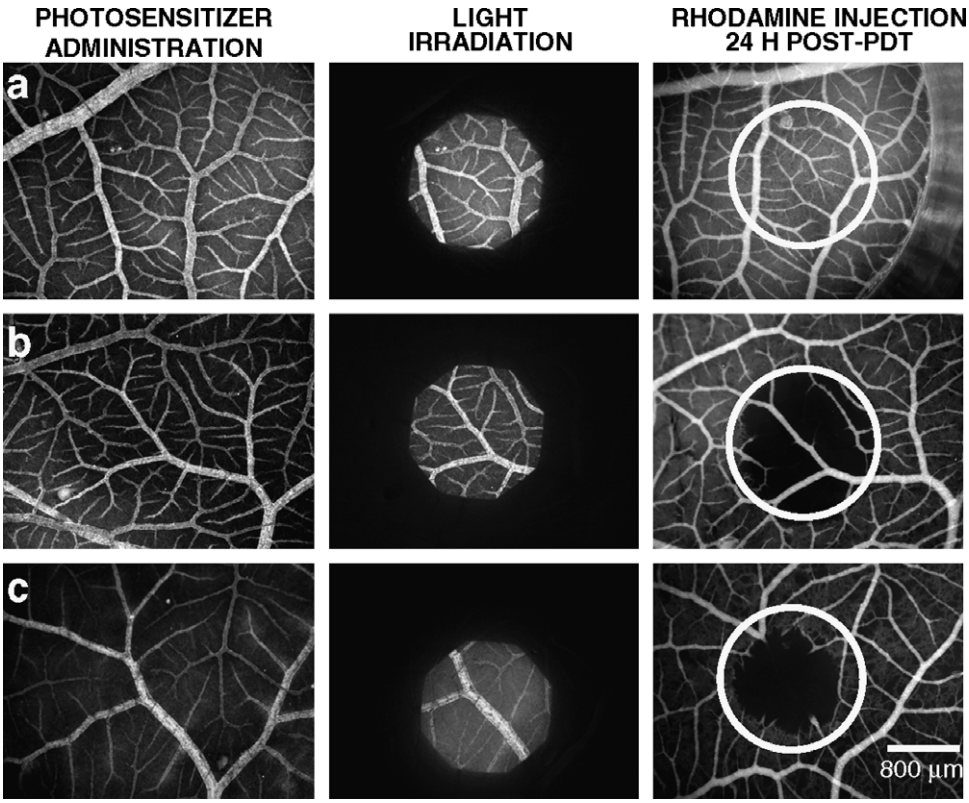

Fig. 2. Three typical examples (a, b, and c) of photodynamic activity experiments on the CAM model. First column: fluorescence angiographies after *m*-THPP administration ($\lambda_{excitation}$ 400–440 nm, $\lambda_{emission}$ 625–675 nm). Second column: angiographies taken during light irradiation (15 J/cm^{2}at 420 nm). Third column: angiographies taken after rhodamine 101 injection 24 h post-PDT ($\lambda_{excitation}$ 510–560 nm, $\lambda_{emission} > 610$ nm). Depending on the diameter of the occluded vessels the experiments were scored as 0: row a; 3: row b; and 5: row c.

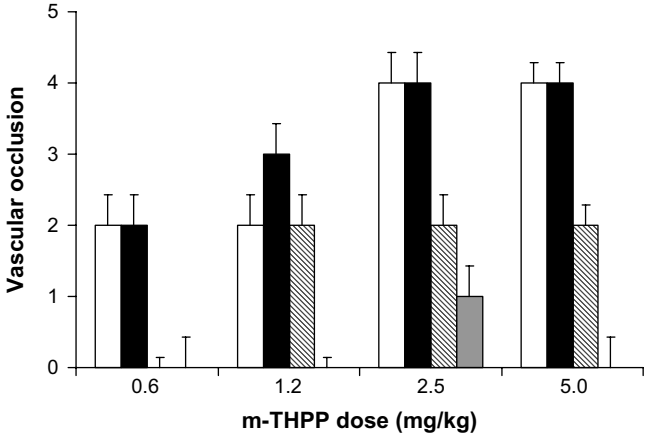

Fig. 3. Vascular occlusion induced by *m*-THPP formulations. Free *m*-THPP (□) and *m*-THPP encapsulated into nanoparticles of 100 nm (■), 300 nm (▨) and 600 nm (▩) were administered in 20 µl, and light irradiation was performed at 15 J/cm^2. Median and MAD ($n = 7$). No significant difference was found between 100 nm NP and free *m*-THPP for all doses. Both 300 nm NP and 600 nm NP had lower activity than free *m*-THPP (exact one-tailed *p*-values <0.01), except for 1.2 mg/kg, where free *m*-THPP and 300 nm NP had similar activity. Significant differences were found within the three sizes of NP at *m*-THPP doses between 1.2 and 5.0 mg/kg (exact two-tailed *p*-values <0.01). At 0.6 mg/kg, 100 nm NP were more active than larger NP (exact two-tailed *p*-values <0.01), but there was no significant difference between 300 and 600 nm NP.

After the injection of *m*-THPP formulations to chick embryos, fluorescence angiographies were taken at several time-points (Fig. 8a and b). Due to *m*-THPP extravasation from CAM vasculature, the normalized C_{phot} steadily decreased after the administration of free *m*-THPP (Fig. 8c). On the contrary, when using NP, *m*-THPP was still primarily localized within the blood vessels 25 min post-administration. T_{max}, which corresponds to the time when the normalized C_{phot} reaches its maximum, was observed at 1 min post-administration for free *m*-THPP and 100 nm NP, at 5 min for 300 nm NP, and at 10 min for 600 nm NP (Fig. 8c).

3.3.2. Confocal microscopy of CAM blood vessels after m-THPP administration

To investigate the uptake of *m*-THPP by endothelial cells of CAM vasculature, the main artery of CAM was resected from the chorioallantoic membrane 10 min after the administration of *m*-THPP formulations to chick embryos. The membrane of the endothelial cells was stained with FITC-Con A, which has been already used as CAM endothelial cells marker [14]. With all the formulations, *m*-THPP signal was observed within the endothelial cells (Fig. 9). However, the intensity of the *m*-THPP signal was the lowest for 600 nm NP.

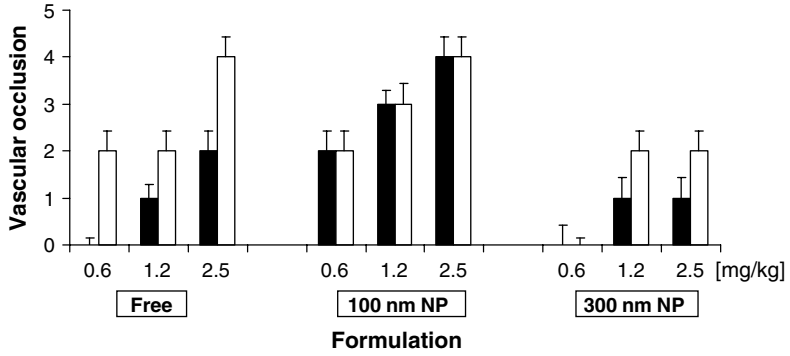

Fig. 4. Influence of the injection volume on the vascular occlusion of CAM vessels. *m*-THPP formulations were administered to chick embryos in a volume of either 10 μl (■) or 20 μl (□), and light irradiation was performed at 15 J/cm^2. Median and MAD ($n = 7$). For free *m*-THPP, a significant difference was found between 10 and 20 μl (exact two-tailed *p*-value <0.01). When NP were used, vascular occlusion was not influenced by the injection volume.

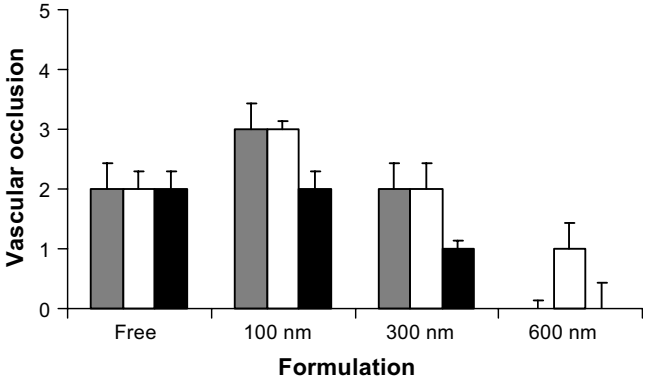

Fig. 5. Activity of *m*-THPP formulations after reconstitution. Formulations (1.2 mg/kg in 20 μl) were administered to chick embryos at different times after reconstitution: immediately (▓), 6 h (□) or 24 h (■) post-reconstitution, and light irradiation was performed at 15 J/cm^2. Median and MAD ($n = 7$). Statistical analyses demonstrate that the activity of both free *m*-THPP and 600 nm remains unaffected for at least 24 h. NP of 100 and 300 nm kept their activity until 6 h post-reconstitution, but had lost activity 24 h post-reconstitution (exact two-tailed *p*-values <0.05).

4. Discussion

4.1. Preparation and characterization of nanoparticles

NP were produced via the emulsification-diffusion technique, which is based on the emulsification of an organic phase containing the polymer, the drug and a solvent partially miscible with water in an aqueous phase containing a stabilizing agent. Mechanical stirring of both phases induces the formation of an oil-in-water nanoemulsion. Upon further addition of water, the organic solvent diffuses from the nanodroplets into the aqueous phase to form the NP after polymer desolvation [15]. The mean size of NP produced by this technique is influenced mainly by the stirring rate, the polymer concentration in the organic phase, and the nature and concentration of the stabilizing agent in the aqueous phase [15,16]. In this study, NP of three sizes were prepared using aqueous phases with different concentrations of the stabilizing agent PVAL. These results are in agreement with previous reports that the increase of PVAL concentration results in the decrease of NP size [15,16]. This technique allowed the production of NP with very low polydispersity indexes (P.I. < 0.1, Table 3), corresponding to NP batches with a homogeneous mean size distribution. Low P.I. are a crucial prerequisite to quantitatively study the influence of NP size on biological effects.

NP relative composition varied depending on the NP size (Table 3). *m*-THPP content slightly increased when the NP size increased due to the decrease of residual PVAL, but the drug to polymer ratio remained essentially unaffected. The residual PVAL percentage was correlated with the initial PVAL concentration used to produce the different NP batches, and increased with decreasing NP size. Higher PVAL contents for smaller NP as compared to larger NP have been already reported [17,18], and might be correlated with the increase of the specific surface area when NP size decreased [19].

4.1.1. Influence of the formulation properties and administration parameters on the photodynamic efficacy of *m*-THPP

The phototoxic effects observed after PDT depend mainly on the PS and oxygen concentration at the target site and on the light dose used for irradiation [1]. In the present study, we have demonstrated that NP size strongly influenced the photodynamic activity of *m*-THPP (Fig. 3). The three batches of NP had similar *m*-THPP loadings and *m*-THPP/PLGA ratios (Table 3). However, the vascular occlusion significantly decreased when increasing the NP size. This effect is in agreement with a recent study evaluating NP made of poly(D,L-lactic acid), loaded with *meso*-tetra(carboxyphenyl)porphyrin, and having diameters ranging from 121 up to 343 nm [20].

The differences observed in vascular occlusion induced by different NP formulations may be explained from various perspectives. NP size can influence the distribution and aggregation state of *m*-THPP within the NP core; the interaction of the encapsulated *m*-THPP with light; the singlet oxygen quantum yield; and the *m*-THPP release

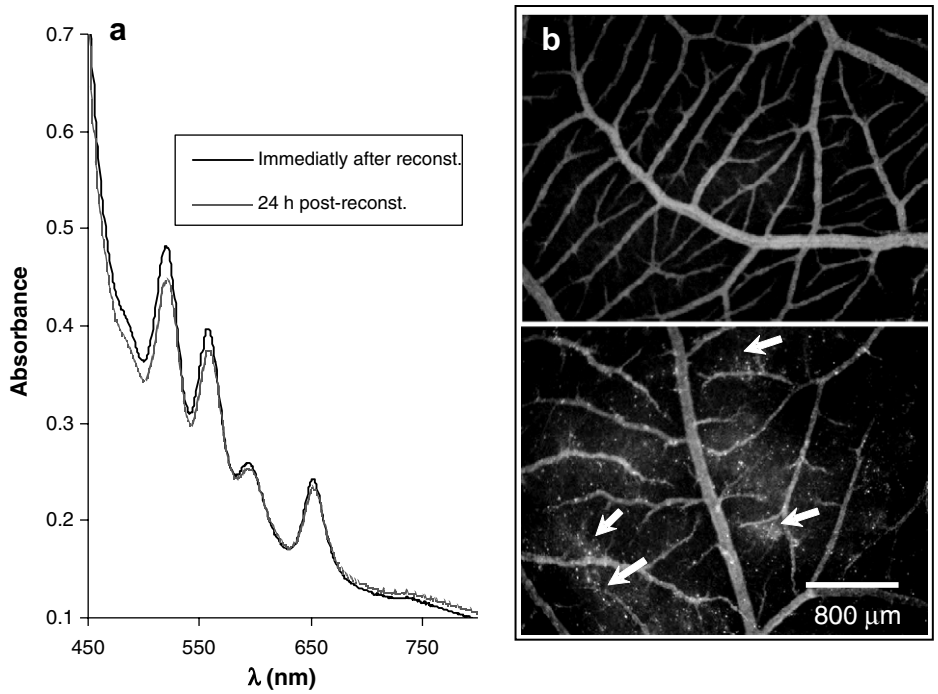

Fig. 6. Effect of reconstitution time on nanoparticle properties. (a) Absorption spectra of porphyrin (10 µg/ml) loaded in 300 nm NP immediately and 24 h after reconstitution. (b) Angiographies of CAM vessels taken 5 min after the administration of 300 nm NP injected either immediately (top) or 24 h after reconstitution (bottom). Notice the presence of fluorescent spots indicated by arrows. Porphyrin dose: 1.2 mg/kg.

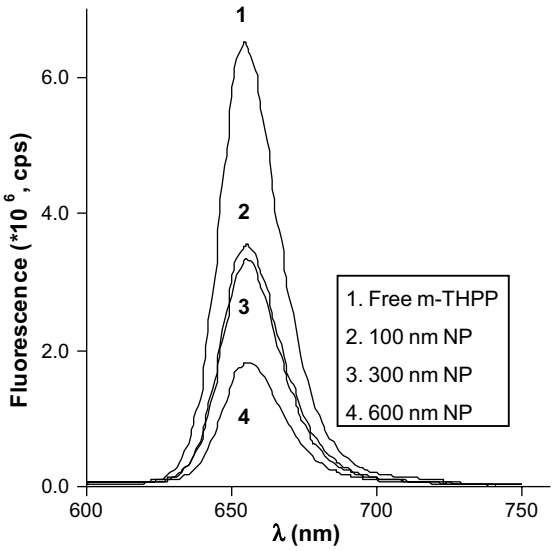

Fig. 7. Fluorescence emission of free *m*-THPP and NP suspended in PBS. *m*-THPP concentration: 5 µg/ml and $\lambda_{excitation}$ 420 nm.

rate. At the biological level, NP size can influence the interaction with blood components, such as opsonization, as well as the uptake by vascular endothelial cells and the tissue distribution. Indeed, size-dependent biodistribution of IV administered colloidal carriers has been already observed in rodents [6,7,21]. Using mice, Fang et al. demonstrated that polymeric NP of 80 nm had longer blood residence time than larger NP, which were taken up by the liver and spleen, organs rich in cells of the mononuclear phagocytic system [22]. The low photodynamic activity observed for large NP in the present study can be related to the higher elimination rate of the large NP compared to that of smaller NP. At day 12 of chick embryo development, reticulum cells in the liver and spleen are functional and are able to take up injected carbon particles [23]. *m*-THPP-loaded NP may have been taken up by the embryo phagocytic system in a size-dependent manner, but biodistribution studies in chick embryo organs should confirm this hypothesis.

Apart from the NP size, the influence of some parameters of administration, such as the injection volume, and the delay between formulation reconstitution and administration, on the efficacy of *m*-THPP was evaluated in this study. The influence of the injection volume was evaluated by administering the same dose of *m*-THPP in a volume of either 10 or 20 µl to chick embryos. As shown in Fig. 4, a higher volume of injection induced an increase in the activity of free *m*-THPP, whereas the activity of *m*-THPP incorporated in NP was independent of the injection volume. The impact of this parameter on free *m*-THPP efficacy might be related to the aggregation state of *m*-THPP. Porphyrins are prone to aggregation in aqueous media [24], and free *m*-THPP was administered in a biocompatible solvent composed of water, PEG 400 and ethanol (5:3:2 v/v/v). Thus, higher *m*-THPP concentrations in smaller volumes can explain the decrease in vascular occlusion, because aggregated forms have reduced photodynamic efficacy, and show different intracellular localization, biodistribution and elimination [25,26]. In contrast to free

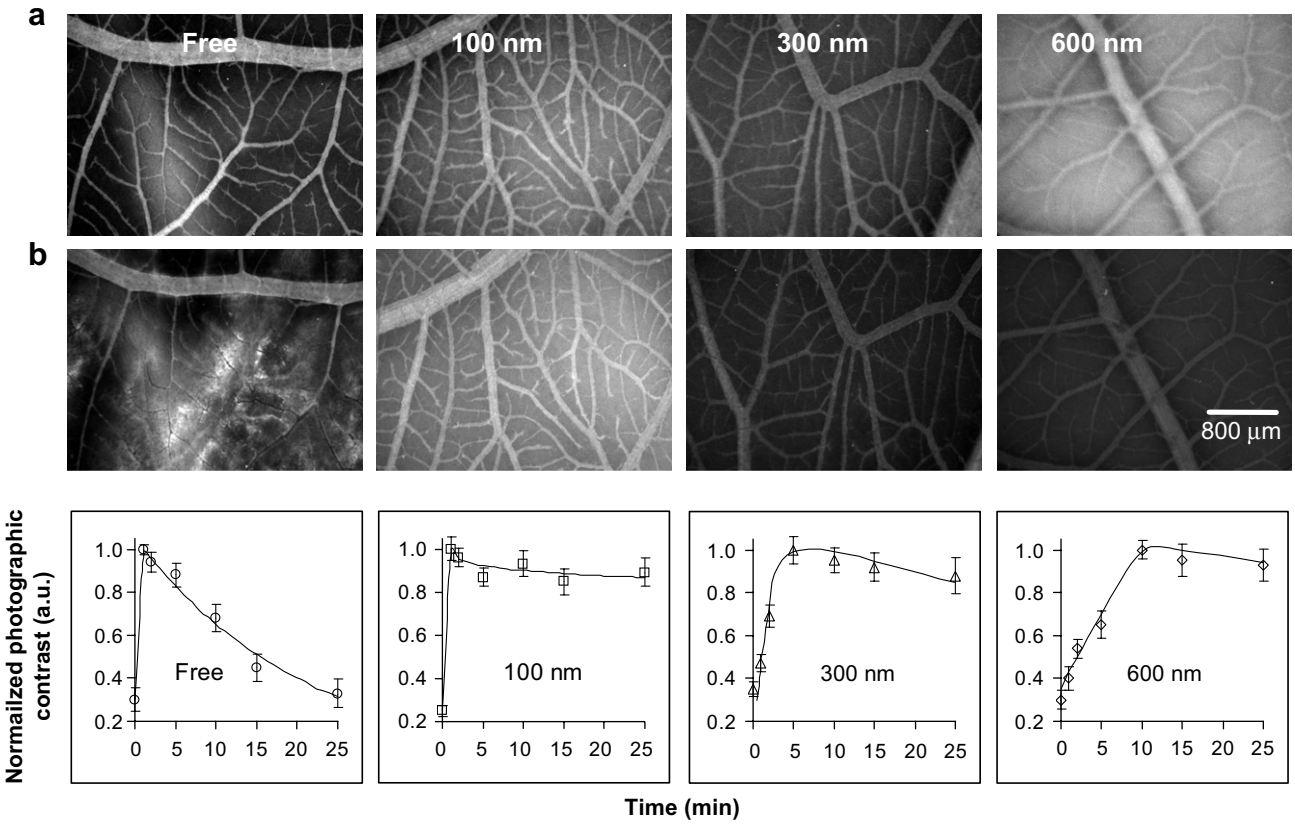

Fig. 8. Photographic contrast after administration of *m*-THPP formulations. Angiographies of CAM vessels taken (a) 1 min and (b) 25 min post-injection (1.2 mg/kg in 20 µl). (c) Evolution of the normalized photographic contrast, which represents *m*-THPP fluorescence within the CAM blood vessels with respect to the fluorescence in surrounding regions. Four embryos were evaluated per formulation (mean ± SD).

m-THPP, the activity of *m*-THPP-loaded NP is independent of the injection volume, emphasizing thus the advantages of using NP. PS aggregation within NP is not influenced by NP concentration in the suspension media. Thus, the activity is independent of the injection or perfusion volumes, and this allows a more efficient control of the PDT outcome. Furthermore, NP show long-term stability as a dry product, and are easily reconstituted as a suspension.

In another series of experiments, the activity of the formulations was evaluated as a function of the delay between formulation reconstitution and administration (Fig. 5). The activity of NP was kept at least 6 h post-reconstitution in PBS. The loss of activity of the 100 and 300 nm NP observed 24 h after reconstitution could be explained by the PS release in the suspension media and subsequent aggregation, as suggested by the decrease in *m*-THPP absorption observed 24 h after NP reconstitution (data for 300 nm NP are shown in Fig. 6a). Furthermore, fluorescence angiographies obtained after the administration of NP kept in suspension for 24 h showed localized spots of high fluorescence intensity, which were not observed when the administration was made immediately or 6 h after reconstitution (Fig. 6b). These results support the hypothesis that the loss of NP activity after long reconstitution times might be related to the *m*-THPP release in the suspension media, as the fluorescent spots were quite similar to those observed in a previous study, when free *m*-THPP was administered [5].

4.2. Influence of biological issues on the photodynamic efficacy of m-THPP

4.2.1. Residence time of m-THPP within the intravascular compartment

We demonstrated that the confinement of *m*-THPP within the vascular space depended on the formulation (Fig. 8a and b). When free *m*-THPP was administered, fast *m*-THPP extravasation was observed, as reported in a previous study [5]. On the contrary, when *m*-THPP was encapsulated in NP, only intravascular *m*-THPP fluorescence was observed. Solid particles cannot cross the vascular endothelium unless it is leaky [6]. Therefore, large NP circulate within the vascular compartment until degradation and/or biodistribution occurs. The size-dependent extravasation of NP from CAM vessels was not observed in our study because the CAM of embryos older than 10 days does not allow the extravasation of molecules larger than 40 kDa (diameter ~9 nm) [27].

The different profiles of the normalized photographic contrast as a function of time observed for the NP formulations (Fig. 8c) can be explained by size-dependent differences in both the fluorescence of circulating NP and

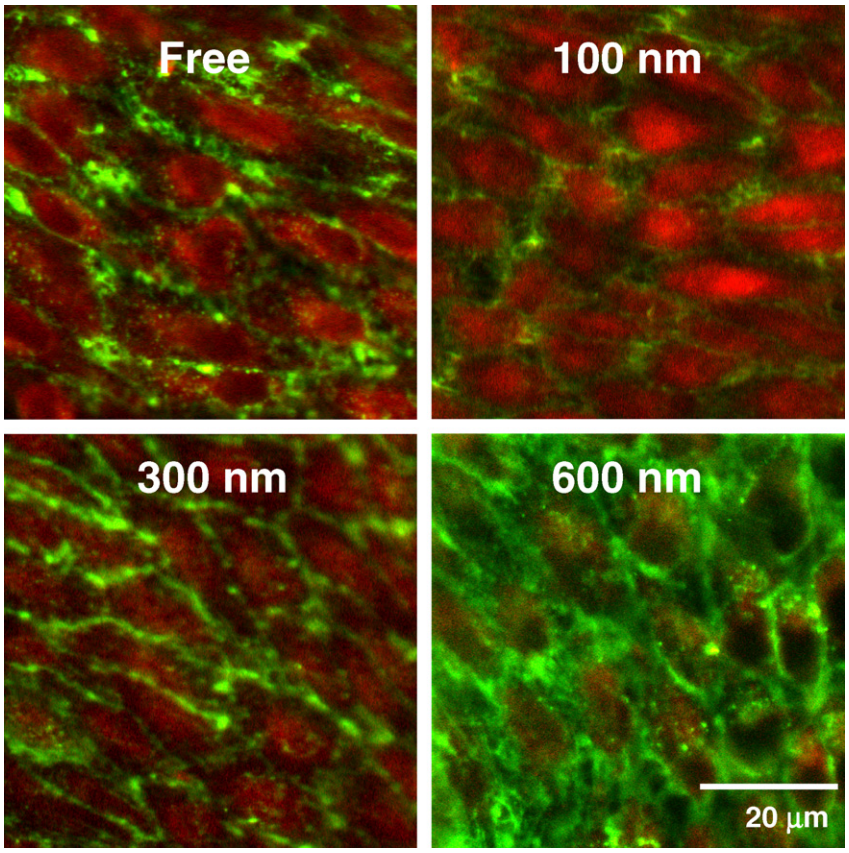

Fig. 9. Confocal images of CAM endothelial vascular cells taken 10 min after administration of *m*-THPP formulations. Cellular membranes were stained with FITC-Con A (green signal, emission: 505–530 nm). *m*-THPP signal was observed within the endothelial cells and is presented in red (emission: 636–753 nm).

the *m*-THPP release rate. As shown in Fig. 7, the *m*-THPP fluorescence after encapsulation decreased with increasing NP size. Additionally, drug release rate has been shown to decrease with increasing NP size [19]. Therefore, in the case of 600 nm NP, the slow increase in fluorescence upon injection and the delayed T_{max} (Fig. 8c) can be explained by a lower *m*-THPP fluorescence concomitant with a slower release rate compared to smaller NP. Since PS activation by light irradiation was performed 1 min after NP injection, a slow *m*-THPP release could explain the lack of activity of *m*-THPP entrapped in large NP (Fig. 3).

4.3. Uptake of m-THPP by vascular endothelial cells

Ten minutes after the administration of the formulations to chick embryos, *m*-THPP signal was observed within endothelial cells of the main artery of CAM demonstrating the endothelial uptake of *m*-THPP when administered encapsulated in NP (Fig. 9). The critical role of NP size in the distribution of particles in vascular tissues has been demonstrated in mammalian models [28,29]. The arterial uptake of NP of around 100 nm was more efficient than that of larger NP. As the endothelial damage following PDT depends on the PS uptake by endothelial cells [3], the low phototoxic effect observed with large NP in this study may be explained by a less efficient uptake by endothelial cells, as suggested by the lower fluorescence intensity observed with large NP (Fig. 9). However, as the intrinsic fluorescence of *m*-THPP loaded in 600 nm NP was low (Fig. 7), *m*-THPP extraction and quantification from CAM vessels could allow verification of this hypothesis.

5. Conclusions

The ability of NP to allow IV administration of hydrophobic PS, as well as the possibility of achieving passive and active targeting, makes NP attractive carriers for PS used in PDT. Furthermore, in this study, it was established that the activity of PS-loaded NP was independent of the volume of administration, and that NP retained their efficacy at least for 6 h after reconstitution.

Considering the main therapeutic applications of PDT, cancer and CNV–AMD, NP of different sizes were developed as a strategy to perform passive targeting. The NP passage to extravascular tissues is considered necessary for optimal cancer treatment, and unwanted for CNV–AMD treatment. It was established that although *m*-THPP -a hydrophobic PS chosen as a model- kept its photodynamic activity after encapsulation, the increase of the NP size was deleterious to the photodynamic efficacy. Based on the

extent of intravascular fluorescence and the PDT experiments, it was demonstrated that for a given PS dose, *m*-THPP will be less available for fluorescence or photodynamic activity when it is incorporated in large NP, than when it is in solution or in small NP. At biological level, the present results suggest that large NP are less active due to a slower *m*-THPP release as evidenced from the delayed T_{max}, and a possible lower uptake by endothelial cells.

Small NP seem to be optimal for PDT cancer treatment due to the EPR effect of tumor tissues, as well as to the high photodynamic efficiency of small NP. For CNV–AMD treatment, the challenge will be to produce NP small enough to enter vascular endothelial cells, but large enough not to cross the fenestrations of the CNV. One possibility that emerges from this observation is the use of small NP coupled to moieties that can actively target the CNV. Recent observations in animal models suggest that the EPR effect occurs in CNV tissues [10], thus passive targeting with small NP containing singlet oxygen scavengers may be used to protect CNV-neighboring tissues from undesired phototoxic effects.

Apart from the biological issues affected by NP size, the extent to which the photochemical properties of PS are affected by encapsulation remains to be determined. Currently, the photochemical properties of *m*-THPP once encapsulated in NP are being characterized.

Acknowledgments

The authors thank Dr. Norbert Lange for his insightful comments and suggestions about this manuscript.

References

[1] T.J. Dougherty, C.J. Gomer, B.W. Henderson, G. Jori, D. Kessel, M. Korbelik, J. Moan, Q. Peng, Photodynamic therapy, J. Natl. Cancer Inst. 90 (1998) 889–905.
[2] R. Klein, B.E. Klein, K.L. Linton, Prevalence of age-related maculopathy. The beaver dam eye study, Ophthalmology 99 (1992) 933–943.
[3] V.H. Fingar, Vascular effects of photodynamic therapy, J. Clin. Laser Med. Surg. 14 (1996) 323–328.
[4] M. Zeisser-Labouèbe, A. Vargas, F. Delie, Nanoparticles for photodynamic therapy of cancer, in: C.S. Kumar (Ed.), Nanomaterials for Cancer Therapy, Vol. 6, Wiley-VCH, Weinheim, 2006, pp. 40–86.
[5] A. Vargas, B. Pegaz, E. Debefve, Y. Konan-Kouakou, N. Lange, J.P. Ballini, H. van den Bergh, R. Gurny, F. Delie, Improved photodynamic activity of porphyrin loaded into nanoparticles: an in vivo evaluation using chick embryos, Int. J. Pharm. 286 (2004) 131–145.
[6] Y. Takakura, R.I. Mahato, M. Hashida, Extravasation of macromolecules, Adv. Drug Deliv. Rev. 34 (1998) 93–108.
[7] D.E. Owens 3rd, N.A. Peppas, Opsonization, biodistribution, and pharmacokinetics of polymeric nanoparticles, Int. J. Pharm. 307 (2006) 93–102.
[8] H. Maeda, The enhanced permeability and retention (EPR) effect in tumor vasculature: the key role of tumor-selective macromolecular drug targeting, Adv. Enzyme Regul. 41 (2001) 189–207.
[9] I. Brigger, C. Dubernet, P. Couvreur, Nanoparticles in cancer therapy and diagnosis, Adv. Drug Deliv. Rev. 54 (2002) 631–651.
[10] H. Kimura, T. Yasukawa, Y. Tabata, Y. Ogura, Drug targeting to choroidal neovascularization, Adv. Drug Deliv. Rev. 52 (2001) 79–91.
[11] N. Lange, J.P. Ballini, G. Wagnieres, H. van den Bergh, A new drug-screening procedure for photosensitizing agents used in photodynamic therapy for CNV, Invest. Ophthalmol. Vis. Sci. 42 (2001) 38–46.
[12] A. Vargas, M. Zeisser-Labouèbe, N. Lange, R. Gurny, F. Delie, The chick embryo and its chorioallantoic membrane (CAM) for the in vivo evaluation of drug delivery systems, Adv. Drug Deliv. Rev. (2007), doi:10.1016/j.addr.2007.04.019.
[13] Y.N. Konan, R. Cerny, J. Favet, M. Berton, R. Gurny, E. Allémann, Preparation and characterization of sterile sub-200 nm meso-tetra(4-hydroxylphenyl)porphyrin-loaded nanoparticles for photodynamic therapy, Eur. J. Pharm. Biopharm. 55 (2003) 115–124.
[14] S.M. Jilani, T.J. Murphy, S.N. Thai, A. Eichmann, J.A. Alva, M.L. Iruela-Arispe, Selective binding of lectins to embryonic chicken vasculature, J. Histochem. Cytochem. 51 (2003) 597–604.
[15] J.C. Leroux, E. Allémann, E. Doelker, R. Gurny, New approach for the preparation of nanoparticles by an emulsification diffusion method, Eur. J. Pharm. Biopharm. 41 (1995) 14–18.
[16] S. Galindo-Rodriguez, E. Allémann, H. Fessi, E. Doelker, Physicochemical parameters associated with nanoparticle formation in the salting-out, emulsification-diffusion, and nanoprecipitation methods, Pharm. Res. 21 (2004) 1428–1439.
[17] S. Galindo-Rodriguez, E. Allémann, E. Doelker, H. Fessi, Versatility of three techniques for preparing ibuprofen-loaded methacrylic acid copolymer nanoparticles of controlled sizes, J. Drug Deliv. Sci. Technol. 15 (2005) 347–354.
[18] Y.N. Konan-Kouakou, R. Boch, R. Gurny, E. Allémann, In vitro and in vivo activities of verteporfin-loaded nanoparticles, J. Control. Release 103 (2005) 83–91.
[19] E. Allémann, J.-C. Leroux, R. Gurny, E. Doelker, In vitro extended-release properties of drug-loaded poly(DL-lactic acid) nanoparticles produced by a salting-out procedure, Pharm. Res. 10 (1993) 1732–1737.
[20] B. Pegaz, E. Debefve, J.P. Ballini, Y.N. Konan-Kouakou, H. van den Bergh, Effect of nanoparticle size on the extravasation and the photothrombic activity of meso(p-tetracarboxyphenyl)porphyrin, J. Photochem. Photobiol. B 85 (2006) 216–222.
[21] S.M. Moghimi, A.C. Hunter, J.C. Murray, Long-circulating and target-specific nanoparticles: theory to practice, Pharmacol. Rev. 53 (2001) 283–318.
[22] C. Fang, B. Shi, Y.Y. Pei, M.H. Hong, J. Wu, H.Z. Chen, In vivo tumor targeting of tumor necrosis factor-alpha-loaded stealth nanoparticles: effect of MePEG molecular weight and particle size, Eur. J. Pharm. Sci. 27 (2006) 27–36.
[23] E.M. Janse, S.H. Jeurissen, Ontogeny and function of two non-lymphoid cell populations in the chicken embryo, Immunobiology 182 (1991) 472–481.
[24] F. Ricchelli, Photophysical properties of porphyrins in biological membranes, J. Photochem. Photobiol. B 29 (1995) 109–118.
[25] U. Isele, K. Schieweck, R. Kessler, P. van Hoogevest, H.G. Capraro, Pharmacokinetics and body distribution of liposomal zinc phthalocyanine in tumor-bearing mice: influence of aggregation state, particle size, and composition, J. Pharm. Sci. 84 (1994) 166–173.
[26] R.W. Boyle, D. Dolphin, Structure and biodistribution relationships of photodynamic sensitizers, Photochem. Photobiol. 64 (1996) 469–485.
[27] V. Rizzo, D.O. DeFouw, Macromolecular selectivity of chick chorioallantoic membrane microvessels during normal angiogenesis and endothelial differentiation, Tissue Cell 25 (1993) 847–856.
[28] C.X. Song, V. Labhasetwar, H. Murphy, X. Qu, W.R. Humphrey, R.J. Shebuski, R.J. Levy, Formulation and characterization of biodegradable nanoparticles for intravascular local drug delivery, J. Control. Release 43 (1997) 197–212.
[29] U. Westedt, L. Barbu-Tudoran, A.K. Schaper, M. Kalinowski, H. Alfke, T. Kissel, Deposition of nanoparticles in the arterial vessel by porous balloon catheters: localization by confocal laser scanning microscopy and transmission electron microscopy, AAPS. PharmSci. 4 (2002) E41.